Supporting information

Modulation of redox potentials utilizing the flexible coordination sphere of a penta-coordinate complex in the solid state

Ryo Ohtani*, Yuu Kitamura, Yuh Hijikata, Masaaki Nakamura, Leonard F. Lindoy, Shinya Hayami*

Corresponding authors:

R. Ohtani, ohtani@sci.kumamoto-u.ac.jp

S. Hayami, hayami@sci.kumamoto-u.ac.jp

Experimental section

Synthesis

(dabco-C_n)Br (n = 15, 16, 17, 18; dabco = 1,4-diazabicyclo[2,2,2]octane)

Bulk powders were synthesized according to the method described previously.[1]

$(PPh_4)_2[Mn(N)(CN)_4]\cdot 2H_2O$ (5)

Bulk samples were synthesized according to the method described previously.[2]

$K_2[Mn(N)(CN)_4]\cdot 2H_2O$ (6)

To $(PPh_4)_2[Mn(N)(CN)_4]\cdot 2H_2O$ (1.00 g; 1.13 mmol) in 120 mL of $CHCl_3$ was added a solution of KI (0.37 g; 2.23 mmol) in 120 mL of H_2O. After stirring, the water phase changed to pink. This pink phase was washed with 120 mL $CHCl_3$ three times. The resulting aqueous solution was evaporated to dryness. Yield 23.4 %. Anal. Found (calcd) for $C_4H_4K_2MnN_5O_2$ (287.23): C 16.53 (16.73); H 1.06 (1.40); N 23.84 (24.38)

(dabco-$(CH_2)_{n-1}$-$CH_3)_2[Mn(N)(CN)_4(H_2O)]\cdot xH_2O$ (n = 15 (1), 16 (2), 17 (3) and 18 (4))

A solution of (dabco-C_n)Br (200 mg) in 15 mL of H_2O at 50 °C was added dropwise to $K_2[Mn(N)(CN)_4]\cdot H_2O$ (26 mg) in 5 mL of H_2O and the solution was stirred at the same temperature for 1 h. The resulting solution was cooled and allowed to stand at 5 °C for 1 day. Orange crystals of **1–4** formed. Recrystallization was carried out from H_2O. The crystals were dried in air.

1; Yield 64.4 %. Anal. Found (calcd) for $C_{46}H_{98}MnN_9O_6$ (928.29): C 60.02 (59.52); H 10.64 (10.60); N 13.61 (13.61)

2; Yield 67.5 %. Anal. Found (calcd) for $C_{48}H_{97}MnN_9O_{3.5}$ (910.30): C 63.17 (63.28); H 10.82 (10.73); N 13.68 (13.84)

3; Yield 73.3 %. Anal. Found (calcd) for $C_{50}H_{106}MnN_9O_6$ (984.39): C 61.11 (61.01); H 10.99 (10.85); N 12.56 (12.81)

4; Yield 74.9 %. Anal. Found (calcd) for $C_{52}H_{110}MnN_9O_6$ (1012.45): C 61.69 (61.69); H 10.93 (10.95); N 12.36 (12.45)

[1] R. Engel, J. I. Rizzo, C. Rivera, M. Ramirez, M. L. Huang, D. Montenegro, C. Copodiferro, V. Behaj, M. Thomas, B. Klaritch-vrana and J. F. Engel, *Chem. Phys. Lipids* 2009, **158**, 61.

[2] J. Bendix, K. Meyer, T. Weyhermuller, E. Bill, N. Metzler-Nolte and K. Wieghardt, *Inorg. Chem.* 1998, **37**, 1767.

Physical measurements

Single-crystal X-ray data for **1** were recorded on a Rigaku R-AXIS RAPID 191R diffractometer with

Cu-Kα (λ = 1.54187 Å) and a detector-to-crystal distance of 191 mm. Single-crystal X-ray data for **2–4** were recorded on a Rigaku/MSC Saturn CCD diffractometer with confocal monochromated Mo-Kα (λ = 0.7107 Å) and processed by using Rigaku/CrystalClear software. The structures of **1–3** were solved by direct methods (Sir 2004) and refined by full-matrix least-squares refinement using the SHELXL-2016/6 computer program. The structures of **4** were solved by the Superflip and refined by full-matrix least-squares refinement using the SHELXL97 computer program. The hydrogen atoms were refined geometrically by using a riding model. Both solution and solid state cyclic voltammetries were measured on an Electrochemical Analyzer Model 1200B (BAS) in 0.1 M KCl aqueous solution at room temperature. A standard three-electrode method with glassy carbon as a working electrode, Pt wire counter electrode and Ag/AgCl reference single electrode were used. CV measurements for **1** and **5** in acetonitrile solution were carried out by the same condition using NH_4ClO_4 instead of KCl. The sample concentration was 1 mM, and a scan rate was 50 mV/s. Differential scanning calorimetry (DSC) thermal analysis was carried out at 10 K min^{-1} on a SHIMADZU DSC50. Elemental analyses (C,H,N) were carried out on a J-SCIENCE LAB JM10 analyzer at the Instrumental Analysis Centre of Kumamoto University.

DFT calculations

All geometry optimizations with fixed angles, θ_a or θ_b were carried out by M06-2X functional[3] using Gaussian 09 E.01.[4] Basis set of SDD with replacing core electrons with the effective core potential of the Stuttgart-Dresden-Bonn[5] and 6-311G(d) were employed for Mn and other atoms, respectively. Diffuse functions were added to C in CN and N in N^{3-}. We employed polarizable continuum model to optimize the complex in water environment.[6]

[3] Y. Zhao and D. G. Truhlar, *Theor. Chem. Account* 2008, **120**, 215-241

[4] Gaussian 09, Revision **E.01**, M. J. Frisch, G. W. Trucks, H. B. Schlegel, G. E. Scuseria, M. A. Robb, J. R. Cheeseman, G. Scalmani, V. Barone, B. Mennucci, G. A. Petersson, H. Nakatsuji, M. Caricato, X. Li, H. P. Hratchian, A. F. Izmaylov, J. Bloino, G. Zheng, J. L. Sonnenberg, M. Hada, M. Ehara, K. Toyota, R. Fukuda, J. Hasegawa, M. Ishida, T. Nakajima, Y. Honda, O. Kitao, H. Nakai, T. Vreven, J. A. Montgomery, Jr., J. E. Peralta, F. Ogliaro, M. Bearpark, J. J. Heyd, E. Brothers, K. N. Kudin, V. N. Staroverov, R. Kobayashi, J. Normand, K. Raghavachari, A. Rendell, J. C. Burant, S. S. Iyengar, J. Tomasi, M. Cossi, N. Rega, J. M. Millam, M. Klene, J. E. Knox, J. B. Cross, V. Bakken, C. Adamo, J. Jaramillo, R. Gomperts, R. E. Stratmann, O. Yazyev, A. J. Austin, R. Cammi, C. Pomelli, J. W. Ochterski, R. L. Martin, K. Morokuma, V. G. Zakrzewski, G. A. Voth, P. Salvador, J. J. Dannenberg, S. Dapprich, A. D. Daniels, Ö. Farkas, J. B. Foresman, J. V. Ortiz, J. Cioslowski and D. J. Fox, Gaussian, Inc., Wallingford CT, 2009.

[5] J. H. Bak, V. D. Le, J. Kang, S. H. Wei and Y. H. Kim, *J. Phys. Chem. C* 2012, **116**, 7386.

[6] J. Tomasi, B. Mennucci and R. Cammi, *Chem. Rev.* 2005, **105**, 2999.

Table S1. Crystallographic data for **1–4**

	1	**2**	**3**	**4**
Formula	$C_{46}H_{86}MnN_9O_6$	$C_{48}H_{90}MnN_9O_{3.50}$	$C_{50}H_{94}MnN_9O_6$	$C_{104}H_{196}Mn_2N_{18}O_{12}$
Formula weight	928.27	911.29	984.38	2000.68
Crystal system	triclinic	monoclinic	triclinic	triclinic
Space group	P -1	P 1 2/c 1	P -1	P -1
a / Å	8.6453(4)	28.357(5)	8.738(5)	8.8487(16)
b / Å	12.6305(6)	9.3098(15)	12.729(7)	24.716(4)
c / Å	24.8982(11)	21.292(4)	26.657(13)	29.102(4)
α / °	77.3723(14)	90.0000	98.635(10)	68.912(8)
β / °	88.5488(12)	104.394(3)	90.561(9)	85.294(15)
γ / °	81.1321(13)	90.0000	99.085(12)	85.972(17)
V / Å^3	2621.2(2)	5444.6(16)	2893(3)	5912.7(17)
Z	2	4	2	2
T / K	223	223	223	223
R1	5.00	6.83	8.37	9.69
wR2	12.75	20.44	22.35	25.40
G.O.F	1.073	1.036	0.982	1.114

Table S2. Structural parameters for **1–4**

	1	**2**	**3**	**unit A in 4**	**unit B in 4**
Mn–N / Å	1.523 (2)	1.523 (3)	1.526 (4)	1.531 (3),	1.526 (3)
Mn–O / Å	2.417	2.453	2.466	2.480	2.380
Mn–C / Å	1.995 (2)	1.976 (4)	1.973 (5)	1.980 (3)	1.995 (5)
	1.995 (2)	1.981 (4)	1.993 (5)	1.992 (4)	1.988 (4)
	1.993 (2)	1.989 (3)	1.993 (5)	1.994 (4)	1.990 (4)

	1.989 (2)	1.997 (4)	1.999 (5)	1.997 (5)	1.987 (4)
C–Mn–C / ° (θ_b)	87.1 (1)	87.4 (1)	87.8 (2)	87.2 (2)	87.9 (2)
	88.4 (1)	88.8 (1)	88.1 (2)	87.6 (2)	90.1 (2)
	89.5 (1)	89.0 (1)	89.3 (2)	90.0 (2)	91.4 (2)
	90.5 (1)	89.7 (1)	90.1 (2)	90.4 (2)	86.4 (2)

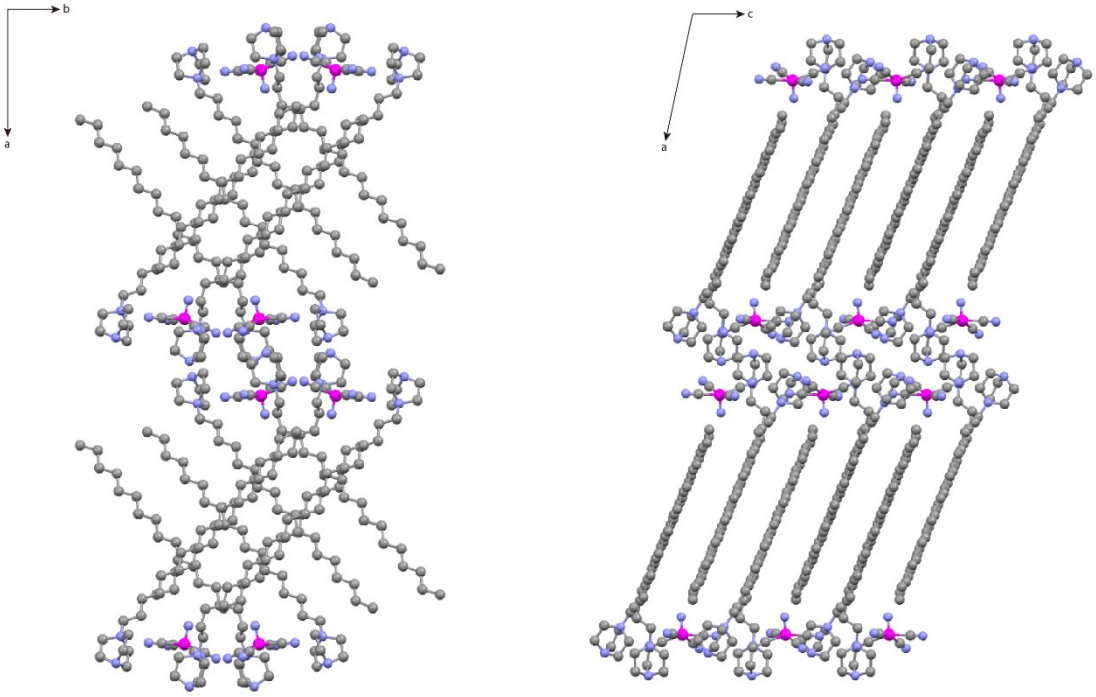

Figure S1. Packing structure of [dabco-$(CH_2)_{17}$-CH_3][Mn(N)$(CN)_4$(dabco-$(CH_2)_{17}$-CH_3)]. (ref. R. Ohtani *et al. Angew. Chem. Int. Ed.* **2015**, 54, 1139-1143)

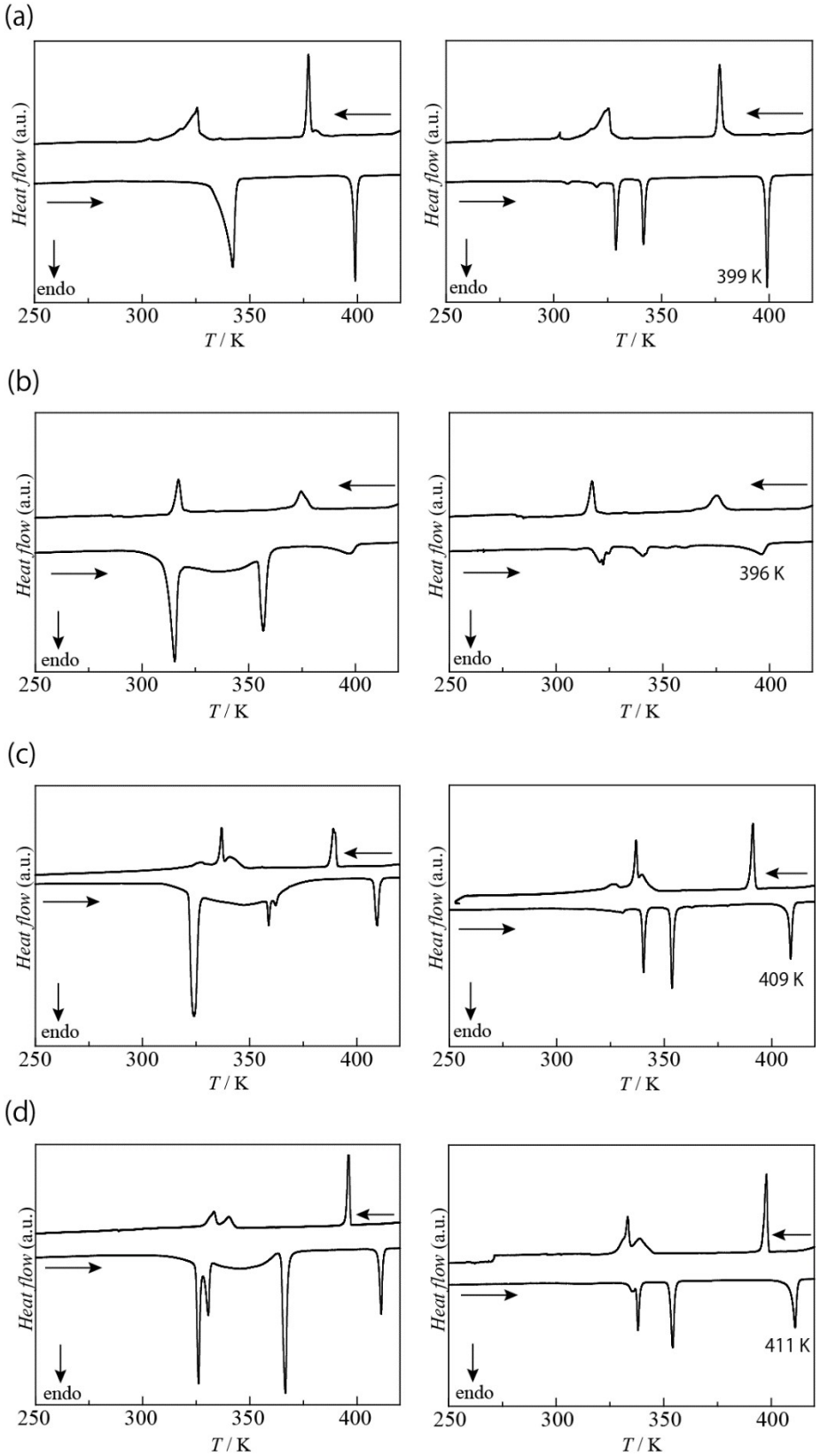

Figure S2. DSC curves for (a) **1**, (b) **2**, (c) **3**, and (d) **4**. Left: 1st scan, right: 2nd scan. The melting

temperatures of **1**, **3** and **4** are 399, 409 and 411 K, respectively. These temperatures increase with increase in alkyl chain length, while **2** melts at 396 K; that is, at a lower temperature than those for the other three. Moreover, in the second run, **1**, **3**, and **4** gave three similar endothermic peaks accompanied by two solid-solid phase transitions and melting. In contrast, the phase transition behavior for **2** is more complicated. These differences unambiguously reflect the different packing structures of the alkyl chains - whether parallel or cross.

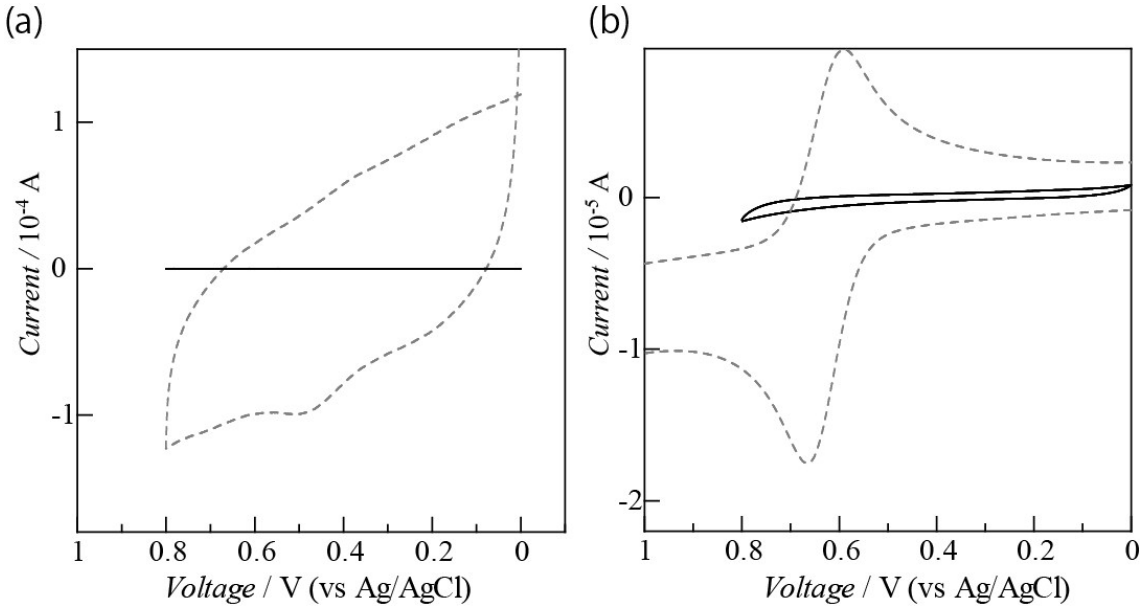

Figure S3. CV results for (a) pristine carbon pastes without Mn complex samples, and for (b) (dabco-C_{15})Br in water. Neither showed peaks in their CV plots. Gray dashed lines in (a) and (b) indicate CV curves for **1** in the solid state, and of **5** in acetonitrile, respectively.

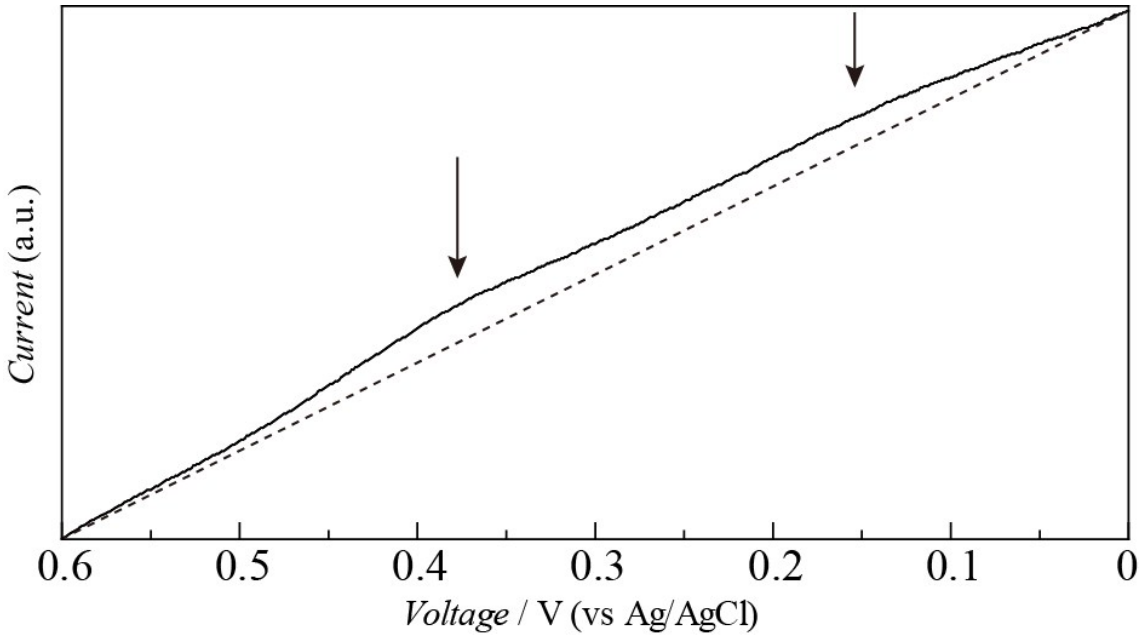

Figure S4. Small peaks observed in the reduction process of CV measurement of **1**.

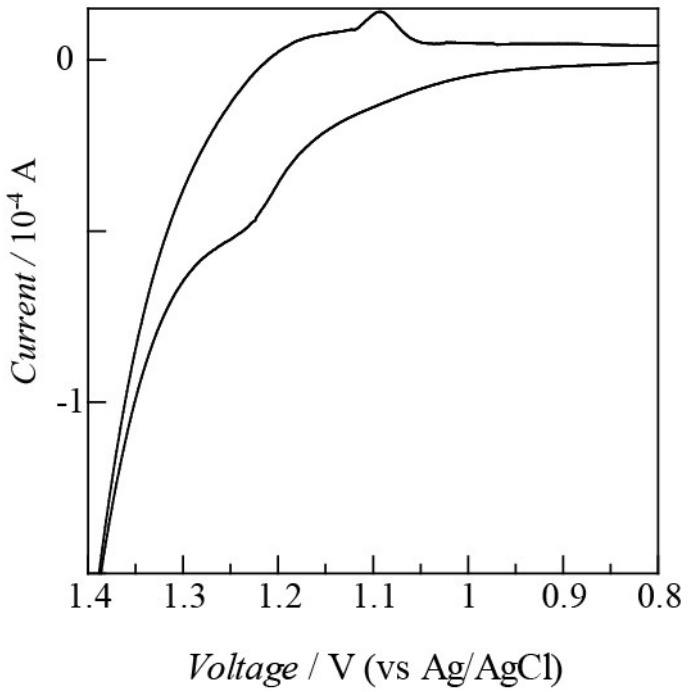

Figure S5. CV curve for **5** in the solid state.

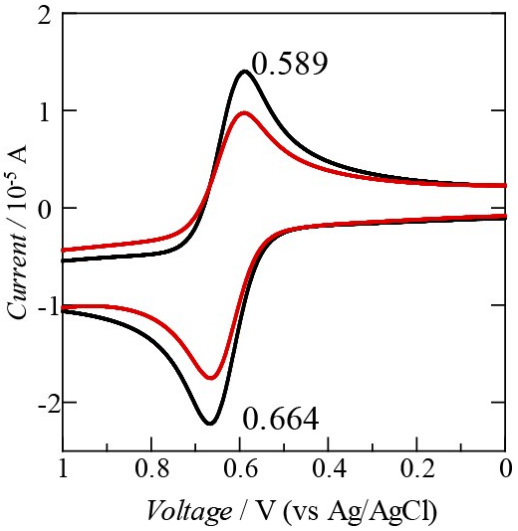

Figure S6. CV curves for **1** (red line) and **5** (black line) in acetonitrile solution.

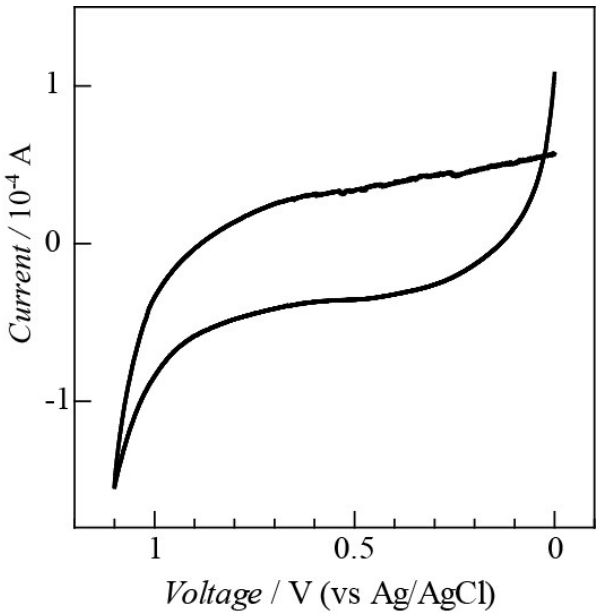

Figure S7. CV curve for **1** after desolvation treatments in the solid state.

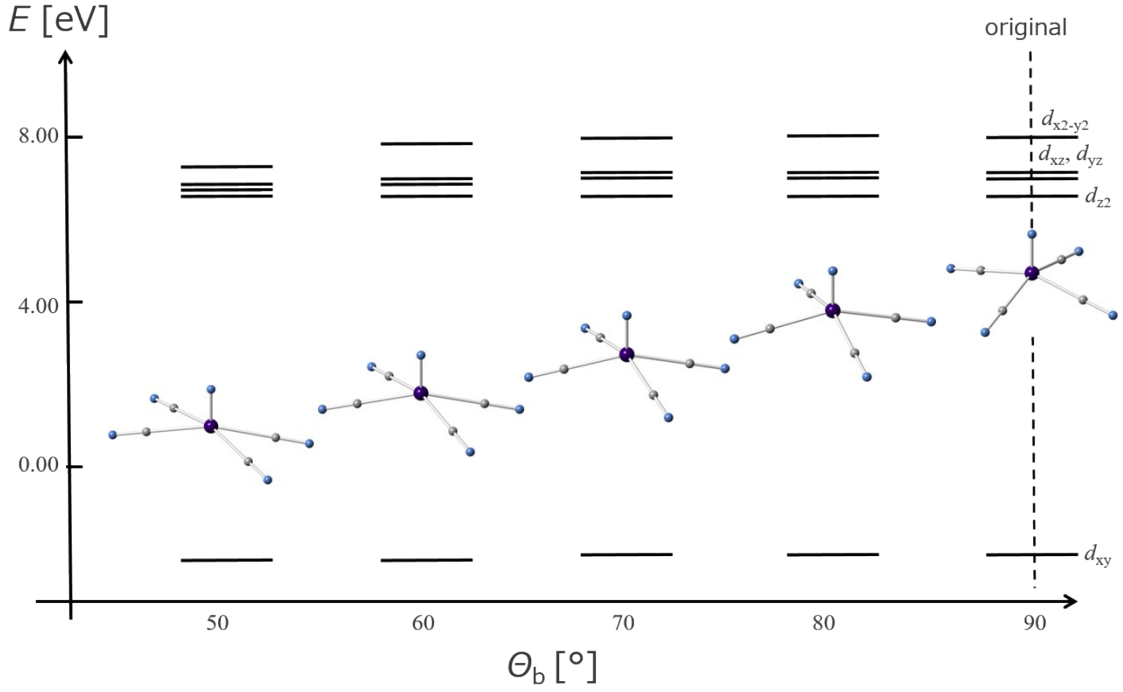

Figure S8. Orbital energy level dependency on the angle θ_b, simulated for in vacuo conditions.

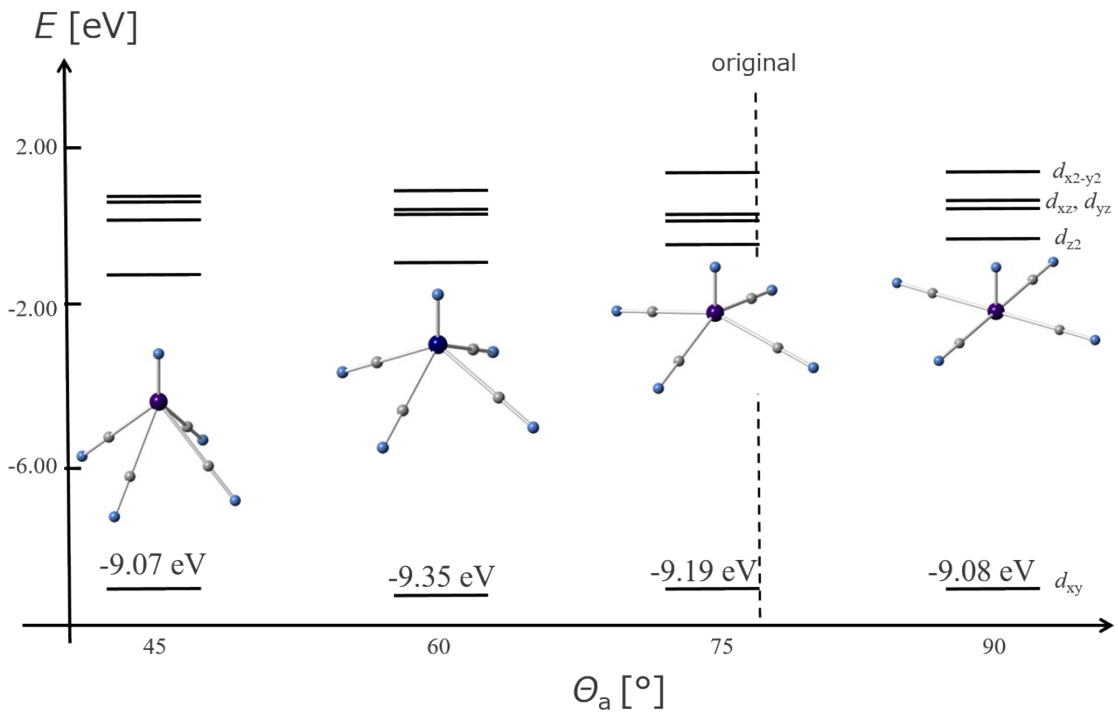

Figure S9. Orbital energy level dependency on the angle θ_a simulated for in water solution.

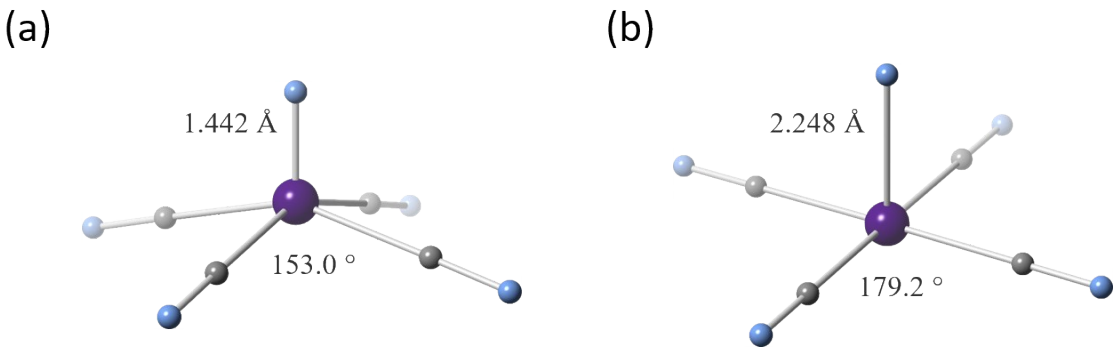

Figure S10. Structures optimized for (a) $[Mn^{V}(N)(CN)]^{2-}$ and (b) $[Mn^{VI}(N)(CN)_4]^{2-}$ in water solution.